Article

Redox–Transmetalation Process as a Generalized Synthetic Strategy for Core–Shell Magnetic Nanoparticles

Woo-ram Lee, Min Gyu Kim, Joon-rak Choi, Jong-Il Park, Seung Jin Ko, Sang Jun Oh, and Jinwoo Cheon

J. Am. Chem. Soc., **2005**, 127 (46), 16090-16097• DOI: 10.1021/ja053659j • Publication Date (Web): 28 October 2005

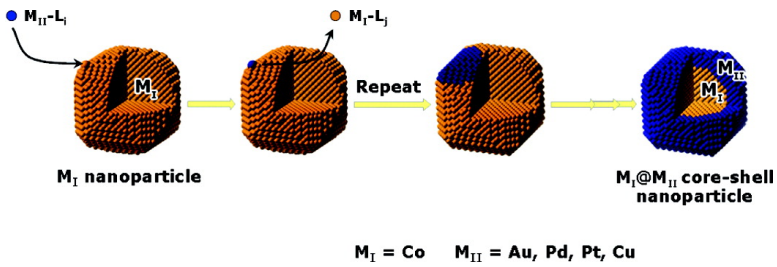

More About This Article

Additional resources and features associated with this article are available within the HTML version:

- Supporting Information
- Links to the 24 articles that cite this article, as of the time of this article download
- Access to high resolution figures
- Links to articles and content related to this article
- Copyright permission to reproduce figures and/or text from this article

View the Full Text HTML

Journal of the American Chemical Society is published by the American Chemical Society. 1155 Sixteenth Street N.W., Washington, DC 20036

J|A|C|S
ARTICLES
Published on Web 10/28/2005

Redox−Transmetalation Process as a Generalized Synthetic Strategy for Core−Shell Magnetic Nanoparticles

Woo-ram Lee,[†] Min Gyu Kim,[‡] Joon-rak Choi,[†] Jong-Il Park,[§] Seung Jin Ko,[†] Sang Jun Oh,[||] and Jinwoo Cheon*,[†]

Contribution from the Department of Chemistry, Yonsei University, Seoul 120-749, Korea, Pohang Accelerator Laboratory (PAL), Pohang 790-784, Korea, Research Institute of Industrial Science and Technology (RIST), Pohang 790-600, Korea, and Korea Basic Science Institute, Daejeon 305-333, Korea

Received June 3, 2005; E-mail: jcheon@yonsei.ac.kr

Abstract: Although multicomponent core−shell type nanomaterials are one of the highly desired structural motifs due to their simultaneous multifunctionalities, the fabrication strategy for such nanostructures is still in a primitive stage. Here, we present a redox−transmetalation process that is effective as a general protocol for the fabrication of high quality and well-defined core−shell type bimetallic nanoparticles on the sub-10 nm scale. Various core−shell type nanomaterials including Co@Au, Co@Pd, Co@Pt, and Co@Cu nanoparticles are fabricated via transmetalation reactions. Compared to conventional sequential reduction strategies, this transmetalation process has several advantages for the fabrication of core−shell type nanoparticles: (i) no additional reducing agent is needed and (ii) spontaneous shell layer deposition occurs on top of the core nanoparticle surface and thus prevents self-nucleation of secondarily added metals. We also demonstrate the versatility of these core−shell structures by transferring Co@Au nanoparticles from an organic phase to an aqueous phase via a surface modification process. The nanostructures, magnetic properties, and reaction byproducts of these core−shell nanoparticles are spectroscopically characterized and identified, in part, to confirm the chemical process that promotes the core−shell structure formation.

Introduction

The fabrication of core−shell nanoparticles is of significance in materials chemistry due to the multifunctionalities and enhanced properties that these structures possess as compared to their mono-elemental counterparts. Multiple functionalities derived from both core and shell components enable them to accomplish versatile roles as optical probes,[1] magnetic separators,[2] and chemical catalysts.[3] Various types of core−shell nanostructures whose core or shell parts consist of metals, semiconductors, and dielectric materials have been prepared.[4] The dual magnetic core−shell nanoparticle system is one that has been successfully studied, and FePt@Fe_3O_4 nanoparticles demonstrate cooperative magnetic switching behaviors through exchange coupling between core and shell materials.[5] Very recently, bifunctional nanoparticles comprised of a magnetic metal core and a semiconductor shell have been reported. In one such example, Co@CdSe nanoparticles combine the properties of magnetic nanoparticles and luminescent semiconductor quantum dots in a core/shell arrangement.[6]

Among the multicomponent nanostructures, in particular, bimetallic core−shell nanoparticles are one of the increasingly important systems due to their enhanced and tunable magnetic, optical, and catalytic properties.[4a−g] Although extensive studies have been conducted to prepare bimetallic core−shell nanoparticles through sequential reduction methods,[7] there tends to be difficulty in producing well-defined bimetallic core−shell nanoparticles, especially with respect to the small magnetic core and thin metallic shell layer required for the total particle size of the sub-10 nm scale regime. Similarly, the precise structural characterization and understanding of the key processes in the

[†] Yonsei University.
[‡] Pohang Accelerator Laboratory.
[§] Research Institute of Industrial Science and Technology.
[||] Korea Basic Science Institute.

(1) Doering, W. E.; Nie, S. *Anal. Chem.* **2003**, *75*, 6171.
(2) Stevens, P. D.; Fan, J.; Gardimalla, H. M. R.; Yen, M.; Gao, Y. *Org. Lett.* **2005**, *7*, 2085.
(3) Son, S. U.; Jang, Y.; Park, J.; Na, H. B.; Park, H. M.; Yun, H. J.; Lee, J.; Hyeon, T. *J. Am. Chem. Soc.* **2004**, *126*, 5026. Zhou, S.; Varughese, B.; Eichhorn, B.; Jackson, G.; McIlwrath, K. *Angew. Chem., Int. Ed.* **2005**, *44*, 4539.
(4) (a) Sobal, N. S.; Ebels, U.; Möhwald, H.; Giersig, M. *J. Phys. Chem. B* **2003**, *107*, 7351. (b) Mandal, S.; Selvakannan, P. R.; Pasricha, R.; Sastry, M. *J. Am. Chem. Soc.* **2003**, *125*, 8440. (c) Mizukoshi, Y.; Fujimoto, T.; Nagata, Y.; Oshima, R.; Maeda, Y. *J. Phys. Chem. B* **2000**, *104*, 6028. (d) Mallik, K.; Mandal, M.; Pradhan, N.; Pal, T. *Nano Lett.* **2001**, *1*, 319. (e) Srnova-Sloufova, I.; Lednicky, F.; Gemperle, A.; Gemperlova, J. *Langmuir* **2000**, *16*, 9928. (f) Sao-Joao, S.; Giorgio, S.; Penisson, J. M.; Chapon, C.; Bourgeois, S.; Henry, C. *J. Phys. Chem. B* **2005**, *109*, 342. (g) Sobal, N. S.; Hilgendorff, M.; Möhwald, H.; Giersig, M.; Spasova, M.; Radetic, T.; Farle, M. *Nano Lett.* **2002**, *2*, 621. (h) Gerion, D.; Pinaud, F.; Williams, S. C.; Parak, W. J.; Zanchet, D.; Weiss, S.; Alivisatos, A. P. *J. Phys. Chem. B* **2001**, *105*, 8861. (i) Zhang, J.; Liu, J.; Wang, S.; Zhan, P.; Wang, Z.; Ming, N. *Adv. Funct. Mater.* **2004**, *14*, 1089.
(5) (a) Zeng, H.; Sun, S.; Li, J.; Wang, Z. L.; Liu, J. P. *Appl. Phys. Lett.* **2004**, *85*, 792. (b) Li, J.; Zeng, H.; Sun, S.; Liu, J. P.; Wang, Z. L. *J. Phys. Chem. B* **2004**, *108*, 14005. (c) Zeng, H.; Li, J.; Wang, Z. L.; Liu, J. P.; Sun, S. *Nano Lett.* **2004**, *4*, 187.
(6) Kim, H.; Achermann, M.; Balet, L.; Hollingsworth, J. A.; Klimov, V. *J. Am. Chem. Soc.* **2005**, *127*, 544.
(7) (a) Schmid, G.; West, H.; Mehles, H.; Lehnert, A. *Inorg. Chem.* **1997**, *36*, 891. (b) Henglein, A. *J. Phys. Chem. B* **2000**, *104*, 2201. (c) Watzky, M. A.; Finke, R. G. *J. Am. Chem. Soc.* **1997**, *119*, 10382. (d) Watzky, M. A.; Finke, R. G. *Chem. Mater.* **1997**, *9*, 3083. (e) Besson, C.; Finney, E. E.; Finke, R. G. *J. Am. Chem. Soc.* **2005**, *127*, 8179. (f) Yu, H.; Gibbons, P. C.; Kelton, K. F.; Buhro, W. E. *J. Am. Chem. Soc* **2001**, *123*, 9198.

10.1021/ja053659j CCC: $30.25

synthesis of bimetallic core−shell nanoparticles have been very limited, partly due to the lack of well-defined model systems and difficulties in analyses of such multilayered nanostructures.

In this article, we examine the general applicability of the redox transmetalation process and the characterization of a variety of bimetallic core−shell systems with superparamagnetism and noble metallic properties. We present a highly effective and generalized synthesis of bimetallic core−shell type magnetic nanoparticles via a redox transmetalation process. Although this method has the potential to be an effective protocol for the fabrication of core−shell nanostructures, there has been only one reported case of Co@Pt.[8] Therefore, in this article, we will focus on the extension of this process to other metals and the general applicability toward various core−shell nanoparticles.

We selected Co nanoparticles as the core material and a combination of materials including gold, palladium, platinum, and copper to comprise the shell layers. In these core−shell structures, the core magnetic component possesses various potential functionalities in areas such as magnetic storage, cell separation vector, and magnetic resonance imaging (MRI). The surface properties of such shell layers can be utilized in roles such as catalysis,[9] surface enhanced Raman scattering (SERS) signal enhancers,[10] conjugation layers with biological molecules,[11] and protective layers.[12]

Experimental Procedures

General Methods. All reactions were carried out under an argon atmosphere using standard airless techniques. $Pd(hfac)_2$ (hfac = 1,1,1,5,5,5-hexafluoroacetylacetonate), $Pt(hfac)_2$, $Cu(hfac)_2$, dodecane isocyanide, and *N,N,N*-trimethyl(11-mercaptoundecyl)ammonium chloride were prepared according to literature methods.[13] Toluene, nonane, and *o*-dichlorobenzene (ODCB) were distilled over sodium, and ethanol was distilled over calcium hydride. Solvents were carefully degassed by a freeze−pump−thaw technique before use. $Co_2(CO)_8$, NaAOT (AOT = bis(2-ethylhexyl)sulfosuccinate), and trioctylphosphine (TOP) were purchased from Strem and Sigma-Aldrich, and $[(C_8H_{17})_4N]^+[AuCl_4]^-$ was obtained from the toluene phase after mixing solutions of $(C_8H_{17})_4N^+Br^-$ in toluene and aqueous $HAuCl_4$ with vigorous stirring.

Synthesis of Nanoparticles. (a) Co Nanoparticles. Co nanoparticles were synthesized by thermal decomposition of dicobalt octacarbonyl ($Co_2(CO)_8$) in the presence of NaAOT following a previously developed method (Figure 1a).[14] A toluene solution containing $Co_2(CO)_8$ (0.5 M, 4 mL) was injected into refluxing 36 mL of a toluene solution containing NaAOT (0.089 g, 0.2 mmol) and cooled to room temperature after 6 h. The 6.5 nm (σ = 0.6 nm) Co nanoparticles were separated by the addition of ethanol and centrifuging, then redispersed in an organic solvent such as toluene.

(b) Co@Au Core−Shell Nanoparticles. Co nanoparticles (14 mg, 0.2 mmol), $[(C_8H_{17})_4N]^+[AuCl_4]^-$ (32.2 mg, 0.04 mmol), and TOP (0.089 mL, 0.2 mmol) were dissolved in 4 mL of ODCB and heated to 180 °C. After 30 min, the solution was cooled to room temperature, and an excess amount of ethanol was added. The black powder was isolated by centrifugation and redispersed in an organic solvent such as toluene. The structure and morphology of the nanoparticles were analyzed by transmission electron microscopy (TEM), high resolution TEM (HRTEM), energy-dispersive X-ray spectroscopic analysis (EDS), and X-ray absorption spectroscopic (XAS) techniques. A metal containing green inorganic byproduct was dried and purified in a silica column and analyzed by elemental and mass analyses. Elemental Anal. Calcd for $C_{48}H_{102}Cl_2CoP_2$: C, 66.18; H, 11.80; Co, 6.77. Found: C, 66.40; H, 12.01; Co, 6.84.

(c) Co@Pd Core−Shell Nanoparticles. A mixture of $Pd(hfac)_2$ (52 mg, 0.1 mmol) and Co nanoparticles (14 mg, 0.2 mmol) was heated at 150 °C for 6 h in a nonane solution containing 0.1 mmol (0.024 mL) of dodecane isocyanide ($C_{12}H_{25}NC$) as a stabilizer. The nanoparticle product was separated by centrifugation after the addition of ethanol. Obtained nanoparticles were analyzed by the same tools mentioned in the previous section. The metal containing reaction byproduct was isolated from an orange supernatant solution and further purified by sublimation under vacuum before being analyzed by UV−vis absorption and infrared spectroscopy. A strong UV−vis absorption band of the byproduct occurs at 300 nm from a $\pi-\pi^*$ transition, and IR analysis shows peaks at 1643 (C═O str), 1612 (C═C str), 1562 (C═O str, C−H bend), 1535 (C═O str, C−H bend), 1481 (C═O str, C−H bend), 1260 (CF_3 str), and 1207 (C−H in plane bend) cm^{-1}.

(d) Co@Pt Core−Shell Nanoparticles. Co@Pt core−shell nanoparticles were synthesized by refluxing Co nanoparticles (14 mg, 0.2 mmol) and $Pt(hfac)_2$ (61 mg, 0.1 mmol) in a nonane solution containing 0.1 mmol (0.024 mL) of dodecane isocyanide ($C_{12}H_{25}NC$) as a stabilizer. Obtained nanoparticles are stable in air and can be redispersed in typical organic solvents. The orange colored byproduct was confirmed as $Co(hfac)_2$ after being separated and analyzed by the same methods described above.

(e) Co@Cu Core−Shell Nanoparticles. NaAOT was dried at 120 °C in a vacuum for 1 h before use. Co@Cu core−shell nanoparticles were obtained from $Cu(hfac)_2$ (48 mg, 0.1 mmol) and Co nanoparticles (14 mg, 0.2 mmol). The reaction proceeded at 140 °C for 2 h in ODCB solution containing 0.1 mmol (44.5 mg) of NaAOT as a capping molecule. The orange colored byproduct was confirmed as $Co(hfac)_2$ after being separated and analyzed by the same methods described above.

(f) Water-Soluble Co@Au via Phase-Transfer Reagent. As synthesized Co@Au nanoparticles (~3 mg, 0.04 mmol) were dissolved in ODCB (10 mL), and *N,N,N*-trimethyl(11-mercaptoundecyl)ammonium chloride (3.3 mg, 0.04 mmol) was added into this solution. After vortexing for 30 min, reddish black precipitates were formed and isolated by centrifugation. The resulting powders were redissolved in the aqueous phase. These nanoparticles are stable in water for several months.

TEM and HRTEM Analysis. The size distribution, morphology, lattice distances, and crystallographic structures of nanoparticles were studied by TEM performed on an EM 912 Omega operated at 120 kV and HRTEM performed on a Hitachi H9000-NAR operated at 300 kV. For the TEM analysis, nanoparticles dissolved in toluene were placed on a TEM grid and allowed to dry in air. A carbon coated nickel grid was used for the sampling of Co@Cu nanoparticles, and a carbon coated copper grid was used for Co@Au, Co@Pt, and Co@Pd nanoparticles.

XAS Measurements. The powdered nanoparticles were mounted in aluminum cells and sealed with polyimide tape (KAPTON-500H, 125 μm thickness). Sample preparations were carried out in an inert glovebox to prevent any oxidation or contamination. Co, Cu, and Pd K-edges and Pt and Au L_{III}-edges X-ray absorption spectra were

(8) (a) Park, J.-I.; Cheon, J. *J. Am. Chem. Soc.* **2001**, *123*, 5743. (b) Park, J.-I.; Kim, M. G.; Jun, Y.-W.; Lee, J. S.; Lee, W.-R.; Cheon, J. *J. Am. Chem. Soc.* **2004**, *126*, 9072.
(9) (a) Reetz, M. T.; Westermann, E. *Angew. Chem., Int. Ed.* **2000**, *39*, 165. (b) Jansat, S.; Gomez, M.; Philippot, K.; Muller, G.; Guiu, E.; Claver, C.; Castillon, S.; Chaudret, B. *J. Am. Chem. Soc.* **2004**, *126*, 1592.
(10) (a) Doering, W.; Nie, S. *J. Phys. Chem. B* **2002**, *106*, 311. (b) Li, X.; Zhang, J.; Xu, W.; Jia, H.; Wang, X.; Yang, B.; Zhao, B.; Li, B.; Ozaki, Y. *Langmuir* **2003**, *19*, 4285.
(11) (a) Park, S.-J.; Taton, A.; Mirkin, C. *Science* **2002**, *295*, 1503. (b) Hong, R.; Emrick, T.; Rotello, V. M. *J. Am. Chem. Soc.* **2004**, *126*, 13572. (c) Maxwell, D. J.; Taylor, J. R.; Nie, S. *J. Am. Chem. Soc.* **2002**, *124*, 9606. (d) Chen, J.; Reed, M. A.; Rawlett, A. M.; Tour, J. M. *Science* **1999**, *286*, 1550. (e) Tseng, G. Y.; Ellenbogen, J. C. *Science* **2001**, *294*, 1293. (f) Joachim, C.; Gimzewski, J. K.; Aviram, A. *Nature* **2000**, *408*, 541.
(12) (a) Chen, M.; Yamamuro, S.; Farrell, D.; Majetich, S. *J. Appl. Phys.* **2003**, *93*, 7551. (b) Guo, Z.; Kumar, C. S. S. R.; Henry, L. L.; Doomes, E. E.; Hormes, J.; Podlaha, E. J. *J. Electrochem. Soc.* **2005**, *152*, D1.
(13) (a) Siedle, A. R.; Newmark, R. A.; Kruger, A. A.; Pignolet, L. H. *Inorg. Chem.* **1981**, *20*, 3399. (b) Bertrand, J. A.; Kaplan, R. I. *Inorg. Chem.* **1966**, *5*, 489. (c) Funck, L. L.; Ortolano, T. R. *Inorg. Chem.* **1968**, *7*, 567. (d) Weber, W. P.; Gokel, G. W. *Tetrahedron lett.* **1972**, *13*, 1637. (e) Tien, J.; Terfort, A.; Whitesides, G. *Langmuir* **1997**, 13, 5349.
(14) (a) Park, J.-I.; Kang, N.-J.; Jun, Y.-W.; Oh, S. J.; Ri, H. C.; Cheon, J.*ChemPhysChem.* **2002**, *3*, 543. (b) King, S.; Hyunh, K.; Tannenbaum, R. *J. Phys. Chem. B* **2003**, *107*, 12097.

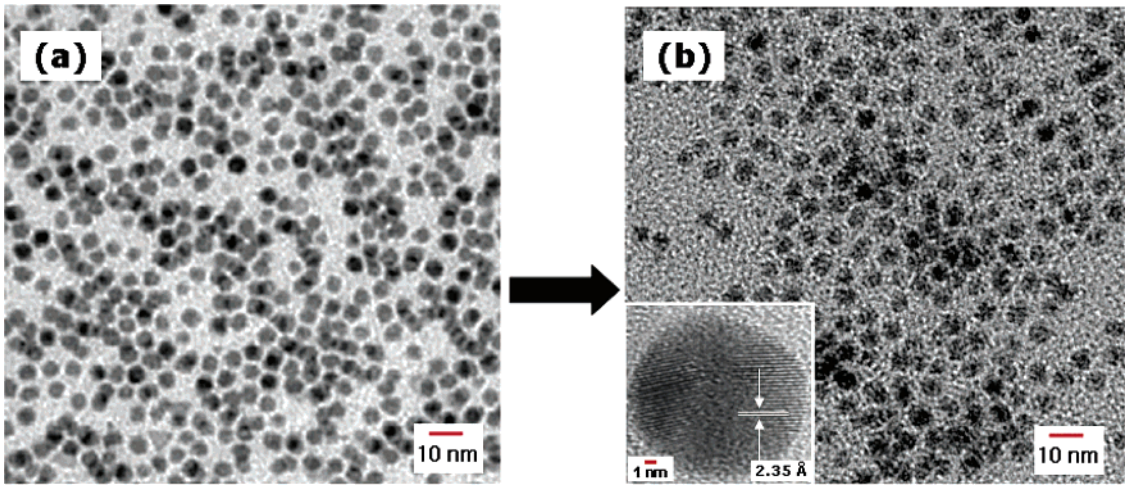

Figure 1. TEM and HRTEM images of (a) 6.5 nm Co nanoparticles and (b) 6.4 nm Co@Au core−shell nanoparticles using Co nanoparticles as the seed material. Lattice distances measured by HRTEM are well-matched to known Au lattice parameters for the (111) plane (inset). The average size of core−shell nanoparticles is ∼6.4 nm, which is similar to the initial size of the Co nanoparticles because the atom exchange process is the only operative reaction.

Scheme 1. Schematic of Core−Shell Nanoparticle Formation via Redox Transmetalation Processes[a]

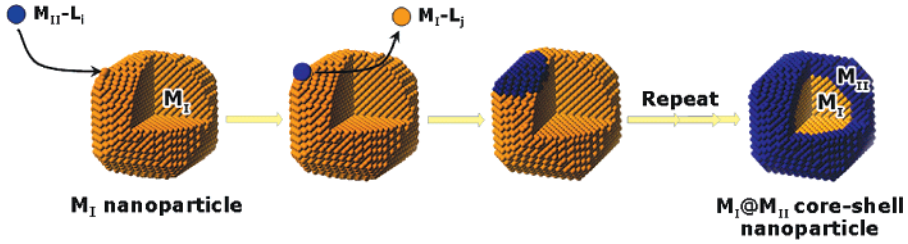

[a] Metal ions (M_{II}) of reactant metal complexes (M_{II}−L_i) are reduced on the surface of M_I nanoparticles while neutral M_I atoms are oxidized to M_I^{y+} by forming a M_I−ligand complex (M_I−L_j) as a resultant reaction byproduct. Repeating this process results in the complete coverage of shell layers on core metals.

recorded on the BL7C beam line of the Pohang light source (PLS) with a ring current of 120−170 mA at 2.5 GeV. A Si(111) double crystal monochromator was employed to monochromatize the X-ray photon energy. The data were collected in transmission mode with nitrogen (85%) and argon (15%) gas-filled ionization chambers as detectors. Higher order harmonic contamination was eliminated by detuning the monochromator to reduce the incident X-ray intensity by ∼30%. Energy calibration was performed using a standard metal foil. The data reduction of the experimental spectra was performed by a standard procedure reported previously.[15] The measured absorption spectra below the pre-edge region were fitted to a straight line, and the background contribution above the post-edge region was chosen using a third-order polynomial fitting. The polynomials of the extrapolated background were subtracted from the total absorption spectra, and the background-subtracted absorption spectra were normalized for a post-edge energy region.

Magnetic Measurements. Magnetic measurements were performed on a SQUID magnetometer (Quantum Design MPMS-7). The hysteresis loops were obtained at 5 and 300 K in a magnetic field varying from +5 to −5 T. The powdered samples were prepared in gelatin capsules in an inert glovebox.

Spectroscopic and Elemental Analysis. UV−vis absorption spectra were obtained with a JASCO V-530 UV/VIS spectrophotometer. Infrared spectra were recorded on an IMPACT 400 FT-IR spectrometer (KBr pellet). Elemental analysis was performed on an inductively coupled plasma atomic emission spectrometer (Shimadzu ICPS-1000III) and elemental analyzer (Flash EA 1112 series/CE Instruments). Mass analysis was performed on an Agilent 5973N mass spectrometer.

(15) Teo, B. K. *EXAFS: Basic Principles and Data Analysis*; Springer-Verlag: Berlin, 1986.

Results and Discussion

When a metal−ligand complex in a positive metal oxidation state ($M_{II}^{x+}L_i^{x-}$) approaches another metal surface (M_I), $M_{II}L_i$ molecules can be reduced through the sacrificial oxidation of the M_I surface atoms to produce M_{II} deposition on the M_I metal surface via a redox transmetalation process (eq 1 and Scheme 1). Since this redox reaction can spontaneously proceed under favorable redox conditions (i.e., the electrochemical potential of the redox reaction (ΔE) is positive) and occurs selectively only on the metal surface to be deposited, this method has been regarded as an efficient route for the selective formation of bimetallic structures.[16] Although such a process is known for bulk scale materials via chemical vapor deposition (CVD) and electroless plating processes, their utilization for nanoscale systems is very rare,[8] and the general applicability of this process has not been examined.

$$n\mathrm{M_I\ (metal\ surface\ atom)} + [\mathrm{M_{II}}]^{x+}[\mathrm{L_i}]^{x-} \rightarrow \mathrm{M_{I(}}_{n-1)\mathrm{@M_{II}}} + [\mathrm{M_I}]^{y+}[\mathrm{L_j}]^{y-} \quad (1)$$

where M = metal, L = ligand, and x and y = oxidation state.

(16) (a) Crane, E.; You, Y.; Nuzzo, R. G.; Girolami, G. S. *J. Am. Chem. Soc.* **2000**, *122*, 3422. (b) Lin, W.; Warren, T. H.; Nuzzo, R. G.; Girolami, G. S. *J. Am. Chem. Soc.* **1993**, *115*, 11644. (c) Gu, S.; Atanasova, P.; Hampden-Smith, M. J.; Kodas, T. T. *Thin Solid Films* **1999**, *340*, 45. (d) Gu, S.; Yao, X.; Hampden-Smith, M. J.; Kodas, T. T. *Chem. Mater.* **1998**, *10*, 2145. (e) Lin, W.; Wiegand, B. C.; Nuzzo, R. G.; Girolami, G. S. *J. Am. Chem. Soc.* **1996**, *118*, 5977. (f) Lin, W.; Nuzzo, R. G.; Girolami, G. S. *J. Am. Chem. Soc.* **1996**, *118*, 5988.

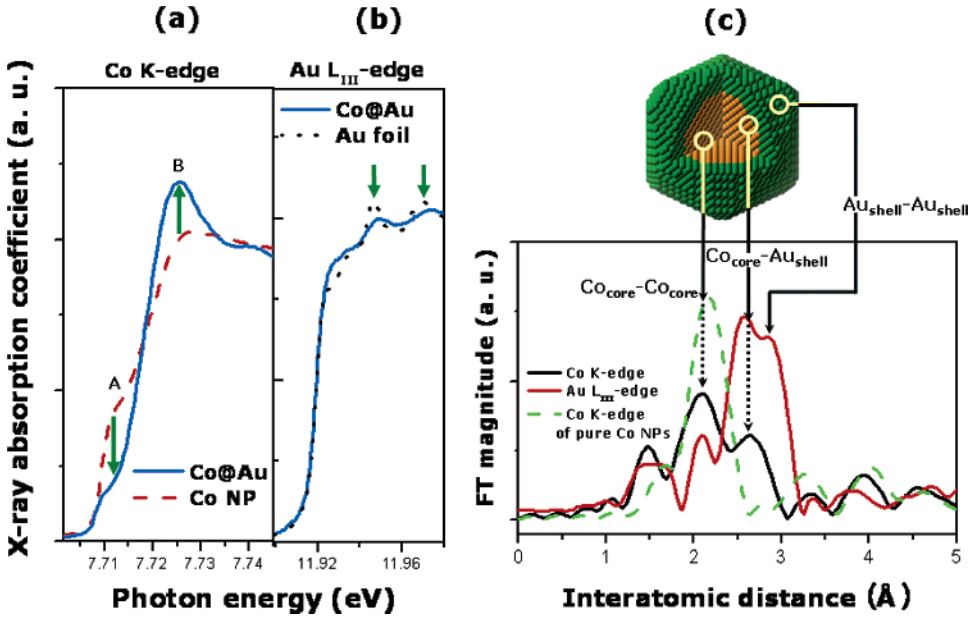

Figure 2. XAS data of Co@Au core−shell nanoparticles. (a) Co K-edge XANES spectra of pure Co nanoparticles and Co@Au nanoparticles. (b) Au L_{III}-edge XANES spectra of bulk Au and Co@Au nanoparticles. (c) Fourier transforms (FTs) for Co K-edge EXAFS spectra (black line) and Au L_{III}-edge EXAFS spectra (red line) of Co@Au nanoparticles and Co K-edge EXAFS spectra of 6.5 nm Co nanparticles (green dotted line), respectively. These data suggest the formation of a cobalt core and a gold shell with an interface layer between them.

Co@Au Core−Shell Nanoparticles. In addition to a cobalt magnetic core, Au has been selected for use as a shell layer since it is particularly important as a platform substrate for self-assembled monolayers (SAM) for applications in molecular electronics and also for colorimetric chemical and biological sensing systems.[11] Co@Au nanoparticles are synthesized by redox transmetalation between surface Co atoms of Co nanoparticles and Au^{3+} ions of $[(C_8H_{17})_4N]^+[AuCl_4]^-$. Co nanoparticles (14 mg, 0.2 mmol) were reacted with $[(C_8H_{17})_4N]^+[AuCl_4]^-$ (32.2 mg, 0.04 mmol) for 30 min at 180 °C in ODCB solvent. After the reaction, pinkish black products were isolated from the reaction solution and analyzed. Monodispersed Co@Au nanospheres are observed by TEM analysis, and the average size was determined to be 6.4 nm (σ = 0.6 nm) (Figure 1b). The size of Co@Au nanoparticles remains similar to that of the starting Co nanoparticles of 6.5 nm. The Co@Au nanoparticle consists of 79 mol % Co and 21 mol % Au according to EDS, and the nanoparticle is estimated to have a 5.7 nm Co core and 0.4 nm Au shell from a simple close packing model considering atomic molar volume, particle diameter, component ratio, and lattice parameter. The formation of Au on Co nanoparticles is also verified by a HRTEM study. According to HRTEM (Figure 1b, inset), the measured lattice distance of 2.35 Å in the surface of nanoparticle is consistent with the known Au lattice parameter (2.355 Å) for the *fcc* (111) plane.

To further validate the core−shell structures of the synthesized bimetallic nanoparticles, we performed XAS analyses. Since XAS is sensitive to atomic local sites and does not depend on the long-range order of the atomic arrangement, it is a powerful technique for analyzing the local structure of these mutlicomponent nanoparticles. The local structures around the Co core and the Au shell atoms of the nanoparticles are investigated by comparing the Co K-edge and Au L_{III}-edge X-ray absorption spectra with that of pure metallic Co nanoparticles and are found to have spectral changes indicative of the local structural variation around the Co atom. Figure 2a,b shows normalized X-ray absorption near-edge structure (XANES) spectra of Co−Au bimetallic nanoparticles (blue solid lines). For the Co K-edge XANES spectrum, a significant change in the intensity of the pre-edge band (peak A) and the white line peak (peak B) as compared to those of pure Co nanoparticles (red dashed line) was observed (Figure 2a). Both the decrease in pre-edge intensity and the increase in white line intensity resulting from electron transfer from Co to Au and population rearrangement between the 3d, 4s, and 4p levels of Co are indicative of the presence of Co−Au chemical interactions. Such results are in good agreement with previous XANES reports of bulk $M_{1-x}Pt_x$ (M = Co and Ni) bimetallic alloys.[8b,17] For the Au L_{III}-edge XANES spectra, the overall peak features beyond the white line become noticeably weaker than that of the Au foil, indicating the formation of its metallic cluster (Figure 2b).[18] Although these XANES spectra show the Co−Au interaction and the existence of Au cluster formation, they are not adequate enough to fully support the formation of a core−shell type structure.

The core−shell structure of the bimetallic Co−Au nanoparticles is supported by the analysis of the Fourier transforms (FTs) of the EXAFS spectra (Figure 2c). For Co K-edge EXAFS spectra, the pure Co nanoparticles show a symmetric FT peak at ~2.2 Å (green dashed line), while there is a new FT peak at ~2.6 Å in addition to one at ~2.2 Å for the Co@Au nanoparticles. These FT peak features suggest that the first shell around the central Co atom includes two different kinds of neighboring atoms of core−shell type nanoparticles. While the shorter FT peak at ~2.2 Å can be assigned to single scattering between inner Co atoms themselves within the core region, the

(17) (a) Hlil, E. K.; Baudoing-Savois, R.; Moraweck, B.; Renouprez, A. J. *J. Phys. Chem.* **1996**, *100*, 3102. (b) Moraweck, B.; Renouprez, A. J.; Hlil, E. K.; Baudoing-Savois, R. *J. Phys. Chem.* **1993**, *97*, 4288.
(18) Lopez-Cartes, C.; Rojas, T. C.; Litran, R.; Martinez-Martinez, D.; de la Fuente, J. M.; Penades, S.; Fernandez, A. *J. Phys. Chem.* **2005**, *109*, 8761.

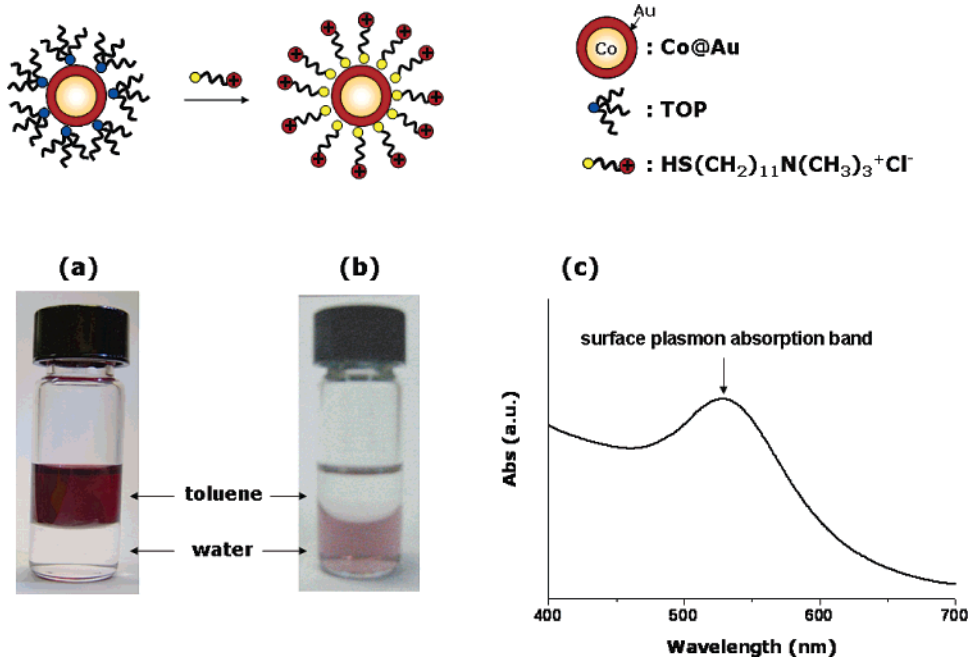

Figure 3. Scheme of ligand exchange by using linker molecules with strong Au−S linkage and high water solubility. Photos taken (a) before and (b) after aqueous phase-transfer reaction. (c) Surface plasmon absorption band at 528 nm in a UV−vis absorption spectrum of water-soluble Co@Au core−shell nanoparticles.

longer FT peak at 2.6 Å corresponds to single scattering between a Co atom in the core surface and a Au atom in the outer shell layer. In the Au L_{III}-edge EXAFS spectra (red line), the FT peaks at ∼2.6 and ∼2.8 Å are due to the scattering between Co_{core} atoms and Au_{shell} atoms in the interface region of Co@Au and the scattering between Au_{shell} atoms and Au_{shell} atoms within the Au shell layer, respectively. The XAS analysis suggests that the obtained nanoparticles are consistent with a Co core and a Au shell nanostructure.

The reaction byproduct data are valuable to support the occurrence of redox transmetalation reactions. The metal containing byproducts analyzed by elemental and mass analyses (see Supporting Information) were identified as $CoCl_2(TOP)_2$. On the basis of our reaction byproduct analysis, the transmetalation reaction between Co nanoparticles and $Au^{3+}$is proposed to be the following (eq 2):

$$10Co + 2[(octyl)_4N]^+[AuCl_4]^- + 6TOP \rightarrow Co_7@Au_2 + 3CoCl_2(TOP)_2 + 2(octyl)_4NCl \quad (2)$$

The expected ratio of Co to Au in the nanoparticle is 7:2 from the formula of $Co_7@Au_2$, and this theoretical ratio is roughly consistent with the observed ratio of 79:21 by EDS.

Water-Soluble Co@Au Core−Shell Nanoparticles. The versatility and robustness of as-prepared Co@Au nanoparticles are tested by aqueous phase transfer experiments. In particular, the aqueous phase transfer of as-prepared Co@Au nanoparticles in organic solvents is of interest since magnetic components containing water soluble Au nanoparticles can be key materials for various biological sensing and detection systems. The phase-transfer process is carried out by replacing the capping ligand, TOP, on the surface of Co@Au with *N*,*N*,*N*-trimethyl(11-mercaptoundecyl)ammonium chloride. Ligand-exchanged Co@Au nanoparticles are obtained in the form of reddish black precipitates by mixing as-synthesized Co@Au nanoparticles (3 mg, 0.04 mmol) in ODCB and *N*,*N*,*N*-trimethyl(11-mercaptoundecyl)ammonium chloride (3.3 mg, 0.04 mmol) for 30 min. Similar phase-transfer processes of nanoparticles from an organic phase into an aqueous phase exist.[19] After the ligand exchange, the core−shell nanoparticles become soluble in water since the hydrophilic cationic part of the surfactant molecule dissolves the nanoparticle in water, while the thiol group of the molecule attaches to the gold shell and stabilizes the nanoparticle (Figure 3). This successful phase transfer of Co@Au nanoparticles is, in part, confirmed by their characteristic magnetic attraction by a typical laboratory magnet and also by the surface plasmon absorption band of the Au shell at 528 nm.

Co@Pd, Co@Pt, and Co@Cu Core−Shell Nanoparticles. Co nanoparticles (14 mg, 0.2 mmol) and $Pd(hfac)_2$ (52 mg, 0.1 mmol) were heated at 150 °C for 6 h in nonane solvent. The Co@Pd nanoparticles with an average diameter of 6.6 nm (σ = 0.8 nm) were observed by TEM (Figure 4a).

The initial reactant molar ratio was 2:1, but the content ratio of the Co@Pd nanoparticle was 1:1 because half of the Co metal was oxidized to the Co^{2+} ion and consumed during the transmetalation reaction. EDS analysis of the nanoparticles supports this with a Co/Pd ratio of 47:53, which is close to the expected 1:1 stoichiometry. The lattice distance measured by HRTEM is 2.24 Å and is congruous with the lattice parameter for the *fcc* (111) plane of Pd (Figure 4a, inset), and $Co_{47}@Pd_{53}$ is estimated to have a 4.9 nm Co core and a 0.9 nm Pd shell. Further structural analyses are conducted by XAS studies.

The reaction byproduct is analyzed by UV−vis and IR spectroscopy (see Supporting Information). The UV−vis absorption from the $\pi-\pi^*$ transition of the hfac ligand, and the observed

(19) (a) Gaponik, N.; Talapin, D. V.; Rogach, A. L.; Eychmuller, A.; Weller, H. *Nano Lett.* **2002**, *2*, 803. (b) Negishi, Y.; Tsukuda, T. *J. Am. Chem. Soc.* **2003**, *125*, 4046. (c) Templeton, A. C.; Hostetler, M. J.; Warmoth, E. K.; Chen, S.; Hartshorn, C. M.; Krishnamurthy, V. M.; Forbes, M. D. E.; Murray, R. W. *J. Am. Chem. Soc.* **1998**, *120*, 4845. (d) Gittins, D. I.; Caruso, F. *Angew. Chem., Int. Ed.* **2001**, *40*, 3001.

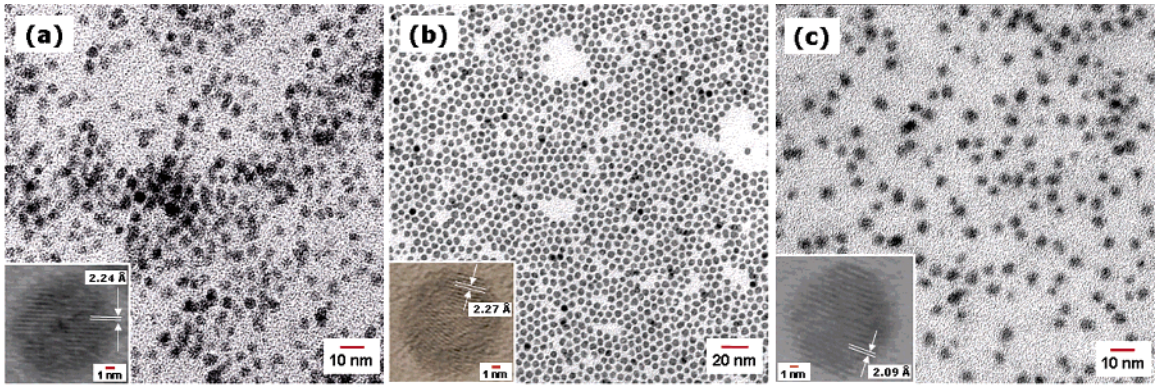

Figure 4. TEM and HRTEM images of (a) 6.6 nm Co@Pd, (b) 6.4 nm Co@Pt, and (c) 6.5 nm Co@Cu core−shell nanoparticles. Measured lattice spacing (inset figures) of 2.24, 2.27, and 2.09 Å by HRTEM are clearly matched to each shell lattice parameters known for the (111) plane of Pd, Pt, and Cu, respectively.

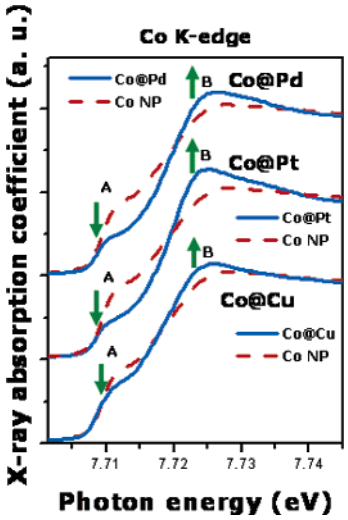

Figure 5. Co K-edge XANES spectra of Co@Pd, Co@Pt, and Co@Cu core−shell nanoparticles.

IR modes are clearly matched with those of $Co(hfac)_2$.[20] Since the major byproduct of this reaction is confirmed as $Co(hfac)_2$, it is reasonable to propose that transmetalation reaction occurs, and the overall reaction is given in eq 3.

$$2Co + Pd(hfac)_2 \rightarrow Co@Pd + Co(hfac)_2 \qquad (3)$$

As developed previously by us, Co@Pt core−shell nanoparticles are also prepared from the reaction between $Pt(hfac)_2$ (61 mg, 0.1 mmol) and Co nanoparticles (14 mg, 0.2 mmol). The 6.4 nm (σ = 0.6 nm) Co@Pt nanoparticles are seen by TEM analysis (Figure 4b). The composition ratio of Co/Pt is 45:55 by EDS, and these nanoparticles are roughly estimated as 4.6 nm Co core and 0.9 nm Pt shell. The inset shows the HRTEM image of the Pt lattice of 2.27 Å, which is consistent with known parameters for the Pt (111) planes. Similarly, the Co@Cu core−shell nanoparticles are obtained from the reaction between $Cu(hfac)_2$ (48 mg, 0.1 mmol) and Co nanoparticles (14 mg, 0.2 mmol). The 6.5 nm (σ = 0.7 nm) Co@Cu nanoparticles are observed by TEM analysis (Figure 4c). The composition ratio of Co/Cu is 54:46 based on EDS. HRTEM analysis shows a lattice distance of 2.09 Å due to the lattice parameter of a *fcc* copper (111) plane, and these core−shell nanoparticles are roughly estimated as 5.2 nm Co core and 0.7 nm Cu shell. Consistent with the case of Co@Pd, the major byproduct is identified for both Co@Pt and Co@Cu cases as $Co(hfac)_2$ by UV−vis absorption and IR analyses[20] (see Supporting Information).

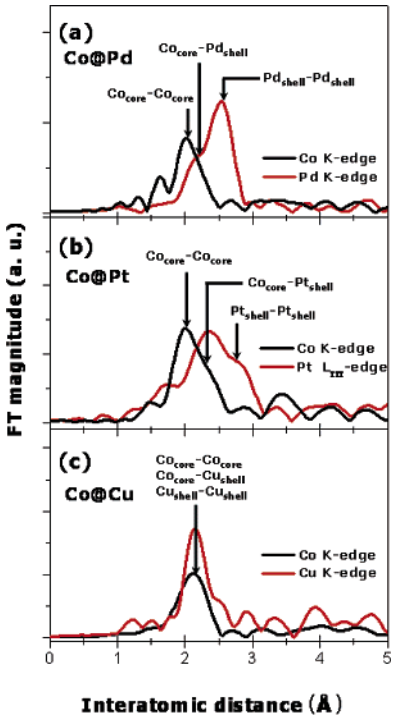

Figure 6. (a) FT peak feature of Co K-edge EXAFS spectra (black line) and Pd K-edge EXAFS spectra (red line) of Co@Pd nanoparticles, (b) FT of Co K-edge (black line) and Pt K-edge (red line) EXAFS spectra of Co@Pt nanoparticles, and (c) FT of Co K-edge (black line) and Cu K-edge (red line) EXAFS spectra of Co@Cu nanoparticles.

Therefore, the transmetalation reaction indeed does occur for all these cases, and the chemical reaction can be summarized as eq 4. During this redox transmetalation process, M^{2+} of $M(hfac)_2$ is reduced on the surface of the Co nanoparticle, while the surface cobalt atom is oxidized to Co^{2+} in the form of $Co(hfac)_2$, and the electron transfer between the two metals results in core−shell type nanoparticles.

$$2Co + M(hfac)_2 \rightarrow Co@M + Co(hfac)_2$$
$$M = Pd, Pt, Cu \qquad (4)$$

(20) (a) Morris, M. L.; Moshier, R. W.; Sievers, R. E. *Inorg. Chem.* **1963**, *2*, 411. (b) Nakamoto, K.; Morimoto, Y.; Martell, A. E. *J. Phys. Chem.* **1962**, *66*, 346. (c) Fackler, J. P., Jr.; Cotton, F. A.; Barnum, D. W. *Inorg. Chem.* **1963**, *2*, 97.

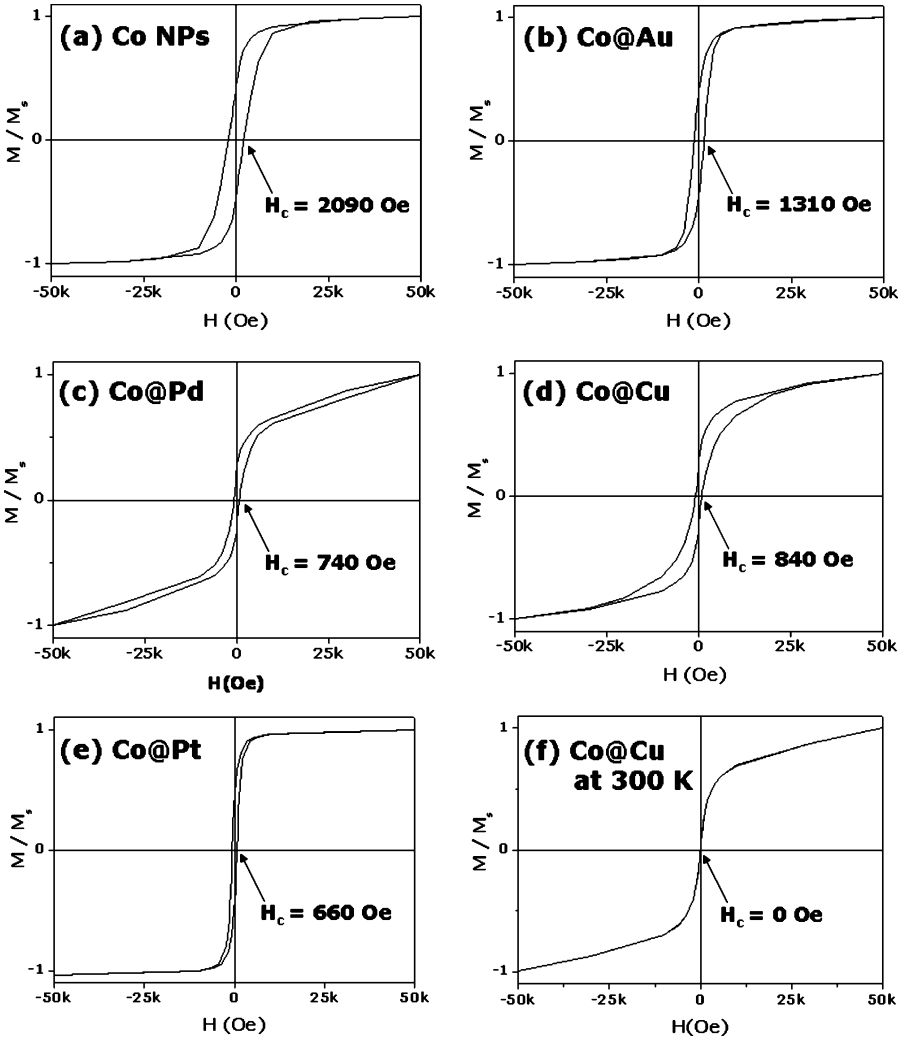

Figure 7. Hysteresis loops of (a) Co nanoparticles and core−shell nanoparticles (b) Co@Au, (c) Co@Pd, (d) Co@Cu, and (e) Co@Pt at 5 K on a SQUID magnetometer. (f) Hysteresis loop of Co@Cu nanoparticles at 300 K shows superparamagnetism.

Core−shell structures of Co@Pd, Co@Pt, and Co@Cu are further confirmed through XAS. When Co K-edge XANES spectra of Co@Pd, Co@Pt, and Co@Cu nanoparticles are compared with that of pure Co nanoparticles, respectively, the intensities of peak A (the pre-edge band) decrease, while those of peak B (the white line peak) increase (Figure 5). These changes show the presence of Co−Pd, Co−Pt, and Co−Cu chemical interactions.

In Figure 6a, FT peaks at ∼2.3 Å for Co K-edge EXAFS spectra and ∼2.2 Å for Pd K-edge EXAFS spectra of Co@Pd nanoparticles reveal the interfacial interaction between Co core atoms and Pd shell atoms, while the peaks at ∼2.0 Å for Co K-edge EXAFS and ∼2.5 Å for Pd K-edge EXAFS result from their core atoms' and shell atoms' own interactions, respectively. Similarly, in the case of Co@Pt, a strong peak at ∼2.0 Å and a shoulder at ∼2.3 Å (Figure 6b, black line) appearing in the FT of the Co K-edge indicates that the first shell around the Co atom includes two different types of neighboring atoms. The peak at ∼2.0 Å is assigned to single scattering by $Co_{core}-Co_{core}$ atoms within the Co_{core} region, and the shoulder at ∼2.3 Å corresponds to single scattering by the $Co_{core}-Pt_{shell}$ at the core−shell interfaces. The FT of the Pt L_{III}-edge EXAFS spectrum (Figure 6b, red line) suggests that three different environments are present for Pt atoms. A strong peak at ∼2.3 Å arising from single scattering of $Co_{core}-Pt_{shell}$ atoms in the interface region is consistently observed, while the shoulder at ∼2.7 Å is due to the $Pt_{shell}-Pt_{shell}$ interaction within the Pt shell layer. For the Co@Cu nanoparticles, although clear FT peak separation is not feasible due to the nearly indistinguishable bond distances of Co−Co and Cu−Cu, it is highly likely that the strong single peaks from Co and Cu K edge, respectively, support the simultaneous presence of Co and Cu with possible core−shell structures (Figure 6c). All these EXAFS data consistently support that the Co@M nanoparticles obtained by this transmetalation reaction are core−shell structures of Co, Pd, Pt, and Cu.

According to our results, the redox transmetalation processes appear to be effective as a general protocol for the fabrication of well-defined bimetallic nanoparticles, while the average diameters of all the core−shell nanoparticles remain similar to that of starting Co nanoparticles. In addition, the calculated standard potential values are 1.80 V for the cell $Co/Co^{2+}//Au^{3+}/Au$, 1.23 V for the $Co/Co^{2+}//Pd^{2+}/Pd$, 1.46 V for the $Co/Co^{2+}//Pt^{2+}/Pt$, and 0.62 V for the $Co/Co^{2+}//Cu^{2+}/Cu$. Since all theoretical redox potential values are positive, redox transmetalation is thermodynamically favorable and experimentally confirmed in the cases of Co@Au, Co@Pd, Co@Pt, and Co@Cu nanoparticles.

Magnetic Measurements. Any possible effects of shell layers on the magnetism of core cobalt are briefly examined by SQUID measurements. Hysteresis loops of the nanoparticles at 5 K show coercivity (H_c) of 2090 Oe for 6.5 nm pure Co nanoparticles, 1310 Oe for Co@Au, 840 Oe for Co@Cu, 660 Oe for Co@Pt, and 740 Oe for Co@Pd core−shell nanoparticles, respectively (Figure 7). The coercivity values of all core−shell nanoparticles are smaller than that of pure Co nanoparticles of 2090 Oe. Considering that the estimated average diameter of cobalt in each type of nanoparticles is 6.5, 5.7, 5.2, 4.7, and 4.9 nm for Co, Co@Au, Co@Cu, Co@Pt, and Co@Pd, respectively, the trend suggests that core−shell nanoparticles with larger Co core sizes have higher coercivity. According to these data, the core magnetic material appears to contribute to the overall magnetism of the core−shell nanoparticles with little, if any, effect on its magnetism from the noble metal shell layer.[6,21] All of these nanoparticles show superparamagnetic behavior at room temperature.

Conclusion

In this paper, we demonstrate the fabrication of various types of core−shell nanomaterials such as Co@Au, Co@Pd, Co@Pt, and Co@Cu through redox transmetalation reactions. Efficient shell growth proceeds on the core metal through the reaction without any additional reducing agent. During the transmetalation processes, metal ions (Au^{3+}, Pd^{2+}, Pt^{2+}, or Cu^{2+}) of the reactant metal complexes are reduced on the surface of Co nanoparticles, while neutral Co atoms are oxidized to Co^{2+} via ligand migration to form a Co−ligand complex as a reaction byproduct. Since shell layer formation and core metal consumption occur simultaneously, the average particle size of the original Co nanoparticles is retained after the reaction process. Although there are slight core size dependent coercivity changes, the room temperature superparamagnetism is clearly well-preserved in all cases. The transfer of Co@Au into the aqueous phase is effective, and the core part of the Co@Au nanoparticles retains its magnetism, while the shell layer of the particles consists of highly versatile gold. We believe that this redox transmetalation strategy can be generally applicable to a variety of core−shell type multimetallic nanoparticle fabrications.

Acknowledgment. We thank Dr. Y. J. Kim (KBSI) for high-voltage TEM (JEM-ARM 1300S), K. T. Son (KBSI) for TEM, and E. M. Kim (KIST) for mass analyses. This work is supported by the Korea Research Foundation (R02-2004-000-10096-0).

Supporting Information Available: EDS spectra of all core−shell nanoparticles, mass data of the reaction byproduct of Co@Au nanoparticles, and spectral analyses of reaction byproducts of Co@Pd, Co@Pt, and Co@Cu nanoparticles. This material is available free of charge via the Internet at http://pubs.acs.org.

JA053659J

(21) Vestal, C. R.; Zhang, Z. J. *Nano Lett.* **2003**, *3*, 1739.